Continuum Mech. Thermodyn.
https://doi.org/10.1007/s00161-018-0623-0

ORIGINAL ARTICLE

Mahdi Zeidi · Chun I. L. Kim

Mechanics of an elastic solid reinforced with bidirectional fiber in finite plane elastostatics: complete analysis

Received: 22 August 2017 / Accepted: 13 January 2018

Abstract A continuum-based model is presented for the mechanics of bidirectional composites subjected to finite plane deformations. This is framed in the development of a constitutive relation within which the constraint of material incompressibility is augmented. The elastic resistance of the fibers is accounted for directly via the computation of variational derivatives along the lengths of bidirectional fibers. The equilibrium equation and necessary boundary conditions are derived by virtue of the principles of virtual work statement. A rigorous derivation of the corresponding linear theory is developed and used to obtain a complete analytical solution for small deformations superposed on large. The proposed model can serve as an alternative 2D Cosserat theory of nonlinear elasticity.

Keywords Finite plane deformations · Fiber-reinforced material · Bidirectional fiber · Superposed incremental deformations · Strain-gradient theory

1 Introduction

The mechanics of fiber-reinforced solids have consistently been the subject of intense study [1,2] that significantly advances our knowledge and practice in materials science and engineering. The subject leads to two major branches of researches involving either the direct investigation of local behaviors of an individual fiber–matrix system including interfacial region or the development of continuum theory through which the overall microscopic behavior of fibers is adequately taken into account in the model of deformations. The former relies on massive identification procedures, which most often require huge computational resources. Nonetheless, this approach was used successfully in the analysis of the mechanics of composite materials (see, for example, [3,4]). Continuum-based approaches offer the advantages of the continuum descriptions and the associated mathematical framework. This presumes the fibers to be densely distributed so as to render meaningful idealization of homogenized fiber–matrix composites. The composite is, therefore, modeled by a special type of anisotropic material in which the response function depends on the conventional deformation gradient, typically augmented by bulk incompressibility and/or fiber inextensibility. In the latter, the resulting prediction models are often so constrained that the final deformed configurations can be determined essentially by their kinematic relations, especially those arise in fibers [5,6].

The continuum theory, which accounts micromechanical effects of fibers on an elastic solid, flexural stiffness in particular, has gained renewed attention in recent years [7]. This includes the computation of the curvature change of the fibers, namely the second gradient of the continuum deformations, through which

Communicated by Andreas Öchsner.

M. Zeidi · C. I. L. Kim (✉)
Department of Mechanical Engineering, University of Alberta, Edmonton, AB T6G 2G8, Canada
E-mail: cikim@ualberta.ca

Published online: 29 January 2018

the "refinement" of the first-order classical continuum theory naturally emerges within the context of the nonlinear strain-gradient theory [8–10] of anisotropic elasticity. Current applications of the general theory are discussed in [11–14], and mathematical aspects of the subject are presented in [15]. The aforementioned works may be used in conjunction with strain-gradient theory, which is also in a period of intense study [16,17]. A general theory for an elastic solid with fiber's resistant to flexure, stretch and twist is presented in [18] with the special restrictions that the director fields are solely expressed by a finite rotation-tensor field. In addition, authors in [19,20] developed second-gradient theory in the analysis of fabric materials and the theory further extended to the study of finite plane deformations of meshed structures [21–26]. However, the majority of the studies have been conducted at a conceptual level and/or, in the case of a single (unidirectional) family of fibers [27,28], little has been devoted to the actual implementation of the theory in relevant problems (including the compatible linear theory), particularly those arise in bidirectional fiber composites.

In this paper, we present a continuum-based model in the analysis of an elastic solid, reinforced with bidirectional fibers, undergoing finite plane deformations. Hence, we assume that the fiber's directors remain in a plane field, with no components in the out of plane direction and the corresponding deformation and all material properties are independent of the out of plane coordinate. The bidirectional fibers are regarded as continuously distributed spatial rods of Kirchhoff type such that the kinematics are based on their position field and a director field [29–31]. Within this setting, we propose an energy density function motivated by the works in [7,32] and successively formulate two-dimensional constitutive equations. More precisely, via the computation of variational derivatives along the lengths of bidirectional fibers and the virtual work statement, the corresponding Euler equilibrium equation is derived in which the constraint of bulk incompressibility is augmented. With the Euler equation satisfied, we present a rigorous derivation of the necessary boundary conditions in the case of bidirectional fibers. In addition, the implementation of the model has been made for the neo-Hookean type of material reinforced with bidirectional fibers and subjected to finite plane deformations. The solution of the resulting coupled partial differential equations (PDEs) is obtained through finite element analysis (FEA). The results are then compared with several experimental data demonstrating that the proposed model successfully predicts the deformed configurations of a crystalline nanocellulose (CNC) fiber composite subjected to three-point bending and also corresponds with the experimental results for T700S carbon–E glass fiber composites [33].

In particular, we develop a complete linear theory of the corresponding model within the description of superposed incremental deformations [34], which also includes the rigorous derivation of the linearized Euler equation, admissible boundary conditions and the augmentation of the material incompressibility. By employing adapted iterative reduction and eigenfunction expansion methods [35–37], an exact analytical solution is obtained describing the mechanics of a bidirectional composite subjected to flexural loads. The obtained solution is smooth and stable throughout the entire domain of interest and, more importantly, demonstrates good agreement with the experiments [33] and the corresponding numerical results for *small* deformation regime. It is noted here that, in the present study, we intentionally exclude the scenario of fiber extensibility for the sake of conciseness and completeness. However, this can be easily accommodated by modifying the proposed energy density function (similar to those illustrated in [32]). Lastly, we mention that the presented model can serve as an alternative 2D Cosserat theory of nonlinear elasticity [8,38–40].

Throughout the paper, we make use of a number of well-established symbols and conventions such as $\mathbf{A}^T$, $\mathbf{A}^{-1}$, $\mathbf{A}^*$ and $tr(\mathbf{A})$. These are the transpose, the inverse, the cofactor and the trace of a tensor $\mathbf{A}$, respectively. The tensor product of vectors is indicated by interposing the symbol $\otimes$, and the Euclidean inner product of tensors $\mathbf{A}$, $\mathbf{B}$ is defined by $\mathbf{A}\cdot\mathbf{B} = tr(\mathbf{A}\mathbf{B}^T)$; the associated norm is $|\mathbf{A}| = \sqrt{\mathbf{A}\cdot\mathbf{A}}$. The symbol $|\cdot|$ is used to denote the usual Euclidean norm of vectors. Latin and Greek indices take values in $\{1, 2\}$ and, when repeated, are summed over their ranges. Lastly, the notation $F_{\mathbf{A}}$ stands for the tensor-valued derivatives of a scalar-valued function $F(\mathbf{A})$.

2 Kinematics and equilibrium equations

In view of [7,32], we propose that the mechanical response of the fiber material is governed by the following strain energy function

$$W(\mathbf{F},\mathbf{G}) = \widehat{W}(\mathbf{F}) + W(\mathbf{G}), \quad W(\mathbf{G}) \equiv \frac{1}{2}C_1(\mathbf{F})\left|\mathbf{g}^1\right|^2 + \frac{1}{2}C_2(\mathbf{F})\left|\mathbf{g}^2\right|^2, \tag{1}$$

where $\mathbf{F}$ is the gradient of the deformation function ($\chi(\mathbf{X})$) and $\mathbf{G}$ is the second gradient of the deformation (i.e., $\mathbf{G} = \nabla\mathbf{F}$). The orientation of particular bidirectional fibers is given by

$$\lambda = |\eta|\,,\ \mu = |\tau|\ \text{and}\ \mathbf{l} = \eta\lambda^{-1},\ \mathbf{m} = \tau\mu^{-1}. \tag{2}$$

where

$$\mathbf{FL} = \lambda\mathbf{l}\ \text{and}\ \mathbf{FM} = \mu\mathbf{m}, \tag{3}$$

and

$$\mathbf{F} = \lambda\mathbf{l}\otimes\mathbf{L} + \mu\mathbf{m}\otimes\mathbf{M},$$

in which $\mathbf{L}$ and $\mathbf{M}$ are the unit tangent to the fiber's trajectory in the reference configuration and $\mathbf{l}$ and $\mathbf{m}$ are their counterparts in the deformed configuration. Equation (3) can be derived by taking the derivative of $\mathbf{r}(s(S)) = \chi(\mathbf{X}(S))$, upon making the identifications $\mathbf{L} = \frac{\mathrm{d}\mathbf{X}}{\mathrm{d}S}$ and $\mathbf{l} = \frac{\mathrm{d}\chi}{\mathrm{d}s}$) and similarly for $\mathbf{M}$. In the present study, we consider initially an orthonormal set of fibers undergoing conformal deformations such that

$$\mathbf{M}\cdot\mathbf{L} = \mathbf{m}\cdot\mathbf{l} = \cos\left(\frac{\pi}{2}\right) = \mathbf{0}. \tag{4}$$

The expression for geodesic curvatures of a parametric curve ($\mathbf{r}(s,u)$) in s and u directions is then obtained from Eq. (3) as

$$\mathbf{g}^1 = \frac{\mathrm{d}^2\mathbf{r}(S)}{\mathrm{d}S^2} = \frac{\mathrm{d}(\frac{\mathbf{r}(S)}{\mathrm{d}S})}{\mathrm{d}S} = \frac{\partial(\mathbf{FL})}{\partial\mathbf{X}}\frac{\mathrm{d}\mathbf{X}}{\mathrm{d}S} = \nabla[\mathbf{FL}]\mathbf{L}, \tag{5}$$

and

$$\mathbf{g}^2 = \frac{\mathrm{d}^2\mathbf{r}(U)}{\mathrm{d}U^2} = \frac{\mathrm{d}(\frac{\mathbf{r}(U)}{\mathrm{d}U})}{\mathrm{d}U} = \frac{\partial(\mathbf{FM})}{\partial\mathbf{X}}\frac{\mathrm{d}\mathbf{X}}{\mathrm{d}U} = \nabla[\mathbf{FM}]\mathbf{M}. \tag{6}$$

The compatibility condition of $\nabla\mathbf{F}$ can be seen as

$$G_{iAB} = F_{iA,B} = F_{iB,A} = G_{iBA}. \tag{7}$$

Further, we introduce the following augmented energy function in order to accommodate the constraint of bulk incompressibility

$$U(\mathbf{F},\mathbf{G},\,p) = W(\mathbf{F},\mathbf{G}) - p(J-1), \tag{8}$$

where J is determinant of $\mathbf{F}$ and p is a Lagrange multiplier field.

Although the variational analysis arising in second-gradient elasticity is a well-established subject [8–10, 41] , its implementation in the mechanics of fiber-reinforced composites, particularly in the case of bidirectional fibers, are barely studied. Here, we reformulate the results for the sake of clarity and completeness, especially the connections between the applied loads and the deformations. The weak form of the equations of equilibrium is given by the virtual work statement

$$\dot{E} = P, \tag{9}$$

where P is the virtual work of the applied loads and the superposed dot refers to the variational derivative;

$$E = \int_{\Omega} U(\mathbf{F},\mathbf{G})\,\mathrm{d}A \tag{10}$$

is the strain energy. Since the conservative loads are characterized by the existence of a potential L such that $P = \dot{L}$, in the present case, the problem of determining equilibrium deformations is reduced to the problem of minimizing the potential energy $E - L$. We then have

$$\dot{E} = \int_{\Omega} \dot{U}(\mathbf{F},\mathbf{G},\,p)\,\mathrm{d}A, \tag{11}$$

where

$$\dot{U}(\mathbf{F},\mathbf{G},\,p) = W_{\mathbf{F}}\cdot\dot{\mathbf{F}} + W_{\mathbf{G}}\cdot\dot{\mathbf{G}} - p\dot{J},$$

and subscripts denote corresponding partial derivatives (e.g., $W_{\mathbf{F}} = \partial W/\partial \mathbf{F}$). It is noted here that the scenario of extensible fibers is excluded from the present study for conciseness (i.e., no variation is induced with respect to λ and μ). However, this can be easily accommodated by modifying the proposed energy density function in Eq. (1).

Using the identity $\dot{J} = J_F \cdot \dot{\mathbf{F}} = \mathbf{F}^* \cdot \dot{\mathbf{F}}$, Eq. (11) becomes

$$\dot{E} = \int_{\Omega} \left[\left(W_{\mathbf{F}} - p\mathbf{F}^* \right) \cdot \dot{\mathbf{F}} + \mathbf{W}_{\mathbf{G}} \cdot \dot{\mathbf{G}} \right] \mathrm{d}A. \tag{12}$$

Also from Eq. (7), $W_{\mathbf{G}} \cdot \dot{\mathbf{G}}$ can be expressed as

$$\frac{\partial W}{\partial G_{iAB}} \dot{G}_{iAB} = \frac{\partial W}{\partial G_{iAB}} u_{i,AB} = \left(\frac{\partial W}{\partial G_{iAB}} u_{i,A} \right)_{,B} - \left(\frac{\partial W}{\partial G_{iAB}} \right)_{,B} u_{i,A}, \tag{13}$$

where $u = \dot{\chi}$ is the induced variation of the position field. Substituting the above into (12) yields

$$\dot{E} = \int_{\Omega} \left[\left(\frac{\partial W}{\partial F_{iA}} - pF^*_{iA} \right) \cdot \dot{F}_{iA} + \left(\frac{\partial W}{\partial G_{iAB}} u_{i,A} \right)_{,B} - \left(\frac{\partial W}{\partial G_{iAB}} \right)_{,B} u_{iA} \right] \mathrm{d}A, \tag{14}$$

Thus, we obtain

$$\dot{E} = \int_{\Omega} \left[\frac{\partial W}{\partial F_{iA}} - pF^*_{iA} - \left(\frac{\partial W}{\partial G_{iAB}} \right)_{,B} \right] \dot{F}_{iA} \mathrm{d}A + \int_{\partial\Omega} \left(\frac{\partial W}{\partial G_{iAB}} u_{i,A} \right) N_B \mathrm{d}S, \tag{15}$$

where $\mathbf{N}$ is the rightward unit normal to the boundary curve $\partial\Omega$ in the sense of the Green–Stoke's theorem. In general, the mechanical responses of the engineering materials are uniform (i.e., $C_i(\mathbf{F}) = C_i$) that Eq. (1) now furnishes

$$W_{\mathbf{G}} \cdot \dot{\mathbf{G}} \ = C_1 \mathbf{g}^1 \cdot \dot{\mathbf{g}}^1 + C_2 \mathbf{g}^2 \cdot \dot{\mathbf{g}}^2, \tag{16}$$

where the expression of $W_{\mathbf{G}}$ can be found as

$$W_{\mathbf{G}} = C_1 \mathbf{g}^1 \otimes \mathbf{L} \otimes \mathbf{L} + C_2 \mathbf{g}^2 \otimes \mathbf{M} \otimes \mathbf{M}. \tag{17}$$

Further, in the case of initially straight fibers (i.e., $\nabla \mathbf{M} = 0, \ \nabla \mathbf{L} = 0$), $\mathrm{Div}(W_{\mathbf{G}})$ reduces to

$$\begin{aligned} \mathrm{Div}(W_{\mathbf{G}}) &= C_1 g^1_{i,B} L_A L_B (\mathbf{e}_i \otimes \mathbf{E}_A) + C_2 g^2_{i,B} M_A M_B (\mathbf{e}_i \otimes \mathbf{E}_A) \\ &= (C_1 g^1_{i,B} L_A L_B + C_2 g^2_{i,B} M_A M_B)(\mathbf{e}_i \otimes \mathbf{E}_A), \\ &\because \quad \left(\frac{\partial W}{\partial G_{iAB}} \right)_{,B} = C_1 g^1_{i,B} L_A L_B + C_2 g^2_{i,B} M_A M_B. \end{aligned}$$

Consequently, Eq. (15) becomes

$$\dot{E} = \int_{\Omega} P_{iA} \dot{F}_{iA} \mathrm{d}A + \int_{\partial\Omega} (C_1 g^1_i L_A L_B + C_2 g^2_i M_A M_B) u_{i,A} N_B \mathrm{d}S, \tag{18}$$

where

$$P_{iA} = \frac{\partial W}{\partial F_{iA}} - pF^*_{iA} - C_1 g^1_{i,B} L_A L_B - C_2 g^2_{i,B} M_A M_B. \tag{19}$$

The corresponding Euler equation is then obtained as

$$P_{iA,A} = 0 \text{ or } \mathrm{Div}(\mathbf{P}) = 0. \tag{20}$$

which hold on Ω.

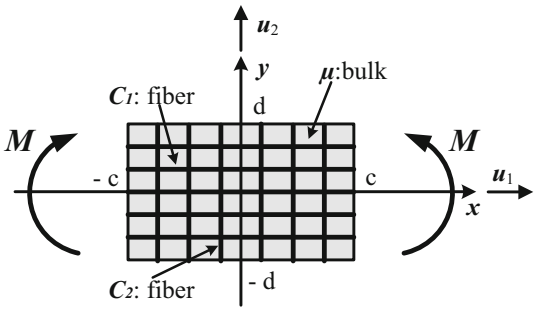

Fig. 1 Schematic of problem

2.1 Example: neo-Hookean materials

The energy density function of the incompressible neo-Hookean materials is given by

$$W = \frac{\mu}{2} tr(\mathbf{C}) = \frac{\mu}{2} tr(\mathbf{F}^T \mathbf{F}) = \frac{\mu}{2} \mathbf{F} \cdot \mathbf{F}. \tag{21}$$

Thus, from Eqs. (19–20), the corresponding Euler equation can be obtained as

$$P_{iA,A} = \mu F_{iA,A} - p_{,A} F^*_{iA} - C_1 g^1_{i,B} L_A L_B - C_2 g^2_{i,B} M_A M_B = 0, \ \because F^*_{iA,A} = 0 \text{ (Piola's identity)}. \tag{22}$$

Now consider a fiber-reinforced material which consists of initially orthonormal set of fibers,

$$\mathbf{L} = \mathbf{E}_1, \quad L_1 = 1, \quad L_2 = 0, \quad \mathbf{M} = \mathbf{E}_2, \quad M_1 = 0, \quad M_2 = 1, \tag{23}$$

and is subjected to plane deformations. Within this prescription, Eq. (22) further reduces to

$$\mu F_{iA,A} - p_{,A} F^*_{iA} - C_1 g^1_{i,11} - C_2 g^2_{i,22} = 0 \text{ for } i, A = 1, 2, \tag{24}$$

where

$$g^1_i = F_{i1,1}, g^2_i = F_{i2,2}, \ F_{iA} = \frac{\partial \chi_i}{\partial X_A} \text{ and } F^*_{iA} = \varepsilon_{ij} \varepsilon_{AB} F_{jB}. \tag{25}$$

In the above, ε_{ij} is the 2-D permutation; $\varepsilon_{12} = -\varepsilon_{21} = 1, \varepsilon_{11} = -\varepsilon_{22} = 0$. Therefore, Eq. (25) together with the constraint of the bulk incompressibility (det $\mathbf{F}$ =1) yields the following coupled PDE system solving for χ_1, χ_2 and p.

$$\begin{aligned} \mu \left(\chi_{1,11} + \chi_{1,22}\right) - p_{,1}\chi_{2,2} + p_{,2}\chi_{2,1} - C_1 \chi_{1,1111} - C_2 \chi_{1,2222} = 0, \\ \mu \left(\chi_{2,11} + \chi_{2,22}\right) + p_{,1}\chi_{1,2} - p_{,2}\chi_{1,1} - C_1 \chi_{2,1111} - C_2 \chi_{2,2222} = 0, \\ \chi_{1,1}\chi_{2,2} - \chi_{1,2}\chi_{2,1} = 1. \end{aligned} \tag{26}$$

Solutions of the above PDE system can be accommodated by commercial packages via FEA (e.g., MATLAB, COMSOL etc…). We reserve the details in "Appendix" for consistency. For demonstration purposes, a set of numerical solutions is obtained for a rectangular composite reinforced with bidirectional fibers (orthonormal) subjected to uniform bending (see Fig. 1). In the simulation, a half problem is considered in which the corresponding boundary conditions are given as $\chi_{1,11} = -M/\mu$, $\chi_{2,11} = 0$, $\chi_2 = 0$ and $\chi_1 = 0$ at $x = 0$, and $\chi_{1,11} = -M/\mu$, $\chi_{2,11} = 0$, $\chi_{2,1} = 0$ and $\chi_{1,1} = 0$ at $x = c$. Similar boundary conditions are employed for the upper ($y = d$) and bottom ($y = -d$) faces except boundary moments where we impose zero moment in order to assimilate flexural deformations (see, [42,43]). The results in Figs. 2 and 3 clearly indicate the effects of the second gradient of the deformations on the resulting deformed configurations.

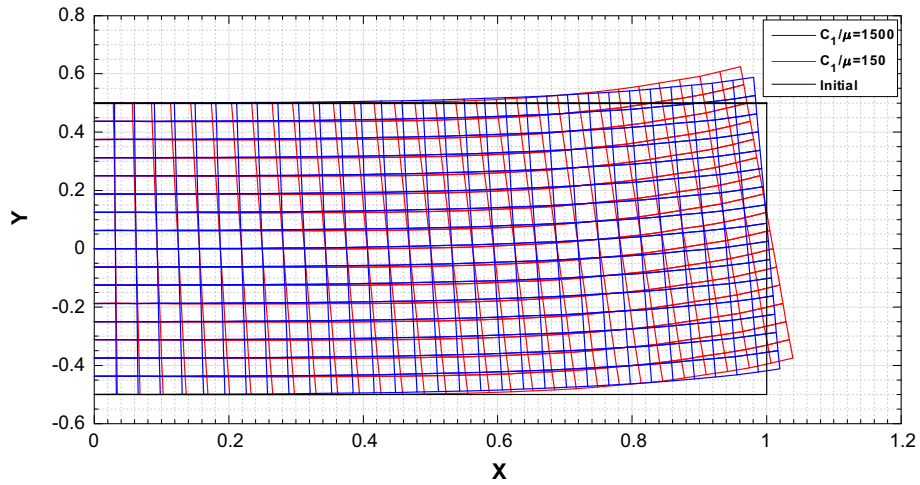

Fig. 2 Deformed configurations with respect to C_1/μ when $M/\mu = 50$ and $C_2/\mu = 100$

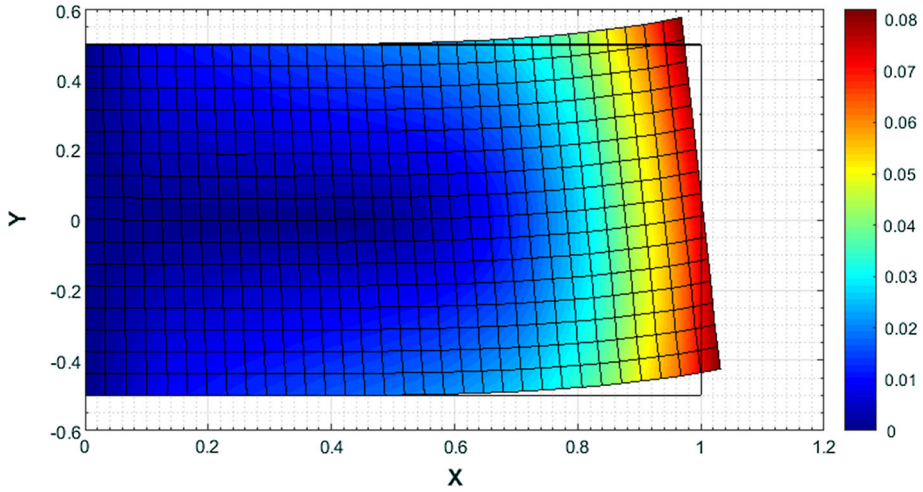

Fig. 3 Deformation contour ($\sqrt{\chi_1^2 + \chi_2^2}$) when $C_1/\mu = 150$, $C_1/\mu = 100$ and $M/\mu = 30$

3 Boundary conditions

Admissible boundary conditions arising from second-gradient continua are well discussed in [44,45]. Here, we reframed the works in the present setting for the sake of consistency and completeness. From Eq. (15), we have

$$\dot{E} = \int_{\Omega} P_{iA}\dot{F}_{iA}\mathrm{d}A + \int_{\partial\Omega}\left(\frac{\partial W}{\partial G_{iAB}}u_{i,A}\right)N_B\mathrm{d}S, \tag{27}$$

where

$$P_{iA} = \frac{\partial W}{\partial F_{iA}} - pF^{*}_{iA} - \left(\frac{\partial W}{\partial G_{iAB}}\right)_{,B}. \tag{28}$$

Decomposing the above as in (13) (i.e., $P_{iA}u_{i,A} = (P_{iA}u_i)_{,A} - P_{iA,A}u_i$) yields

$$\dot{E} = \int_{\partial\Omega} P_{iA}u_iN_A\mathrm{d}S - \int_{\Omega} P_{iA,A}u_i\mathrm{d}A + \int_{\partial\Omega}\left(\frac{\partial W}{\partial G_{iAB}}u_{i,A}\right)N_B\mathrm{d}S, \tag{29}$$

and hence the Euler equation $P_{iA,A} = 0$ which holds in Ω. With this satisfied, Eq. (29) becomes

$$\dot{E} = \int_{\partial\Omega} P_{iA}u_iN_A\mathrm{d}S + \int_{\partial\Omega}\left(\frac{\partial W}{\partial G_{iAB}}u_{i,A}\right)N_B\mathrm{d}S. \tag{30}$$

Now, we make use of the normal–tangent decomposition of $\nabla\mathbf{u}$ as;

$$\nabla\mathbf{u} = \nabla\mathbf{u}(\mathbf{T}\otimes\mathbf{T}) + \nabla\mathbf{u}(\mathbf{N}\otimes\mathbf{N}) = \mathbf{u}'\otimes\mathbf{T} + \mathbf{u}_{,\mathbf{N}}\otimes\mathbf{N}, \tag{31}$$

where $\mathbf{T} = \mathbf{X}'(S) = \mathbf{k}\times\mathbf{N}$ is the unit tangent to $\partial\Omega$. $\mathbf{u}'$ and $\mathbf{u}_{,N}$ are the tangential and normal derivatives of $\mathbf{u}$ on $\partial\Omega$, respectively (i.e., $u_i' = u_{i,A}T_A,\ u_{i,N} = u_{i,A}N_A$). Accordingly, Eq. (30) can be rewritten as

$$\dot{E} = \int_{\partial\Omega} P_{iA}u_i N_A \mathrm{d}S + \int_{\partial\Omega}\frac{\partial W}{\partial G_{iAB}}\left(u_i' T_A N_B + u_{i,N}N_A N_B\right)\mathrm{d}S. \tag{32}$$

Since

$$\frac{\partial W}{\partial G_{iAB}}T_A N_B u_i' = \left(\frac{\partial W}{\partial G_{iAB}}T_A N_B u_i\right)' - \left(\frac{\partial W}{\partial G_{iAB}}T_A N_B\right)' u_i, \tag{33}$$

we obtain

$$\dot{E} = \int_{\partial\Omega}\left\{P_{iA}N_A - \left(\frac{\partial W}{\partial G_{iAB}}T_A N_B\right)'\right\}u_i\mathrm{d}S + \int_{\partial\Omega}\frac{\partial W}{\partial G_{iAB}}u_{i,N}N_A N_B\mathrm{d}S + \int_{\partial\Omega}\left(\frac{\partial W}{\partial G_{iAB}}T_A N_B u_i\right)'\mathrm{d}S. \tag{34}$$

In view of Eq. (17) (i.e., $W_{\mathbf{G}} = C_1\mathbf{g}^1\otimes\mathbf{L}\otimes\mathbf{L} + C_2\mathbf{g}^2\otimes\mathbf{M}\otimes\mathbf{M}$), Eq. (34) furnishes

$$\begin{aligned}\dot{E} = &\int_{\partial\Omega}\left\{P_{iA}N_A - \left(C_1 g_i^1 L_A T_A L_B N_B + C_2 g_i^2 M_A T_A M_B N_B\right)'\right\}u_i\mathrm{d}S\\ &+ \int_{\partial\Omega}(C_1 g_i^1 L_A N_A L_B N_B + C_2 g_i^2 M_A N_A M_B N_B)u_{i,N}\mathrm{d}S\\ &- \sum\left\|(C_1 g_i^1 L_A T_A L_B N_B + C_2 g_i^2 M_A T_A M_B N_B)u_i\right\|,\end{aligned} \tag{35}$$

where the double bar symbol refers to the jump across the discontinuities on the boundary $\partial\Omega$ (i.e., $\|*\| = (*)^+ - (*)^-$) and the sum refers to the collection of all discontinuities. Further, the principle of virtual work ($\dot{E} = P$) states that the admissible mechanical powers take the following form

$$P = \int_{\partial\Omega_t} t_i u_i \mathrm{d}S + \int_{\partial\Omega} m_i u_{i,N}\mathrm{d}S + \sum f_i u_i. \tag{36}$$

Consequently, by comparing Eqs. (35) and (36), we obtain

$$\begin{aligned}\mathbf{t} &= \mathbf{PN} - \frac{\mathrm{d}}{\mathrm{d}S}\left[C_1\mathbf{g}^1(\mathbf{L}\cdot\mathbf{T})(\mathbf{L}\cdot\mathbf{N}) + C_2\mathbf{g}^2(\mathbf{M}\cdot\mathbf{T})(\mathbf{M}\cdot\mathbf{N})\right],\\ \mathbf{m} &= C_1\mathbf{g}^1(\mathbf{L}\cdot\mathbf{N})^2 + C_2\mathbf{g}^2(\mathbf{M}\cdot\mathbf{N})^2,\\ \mathbf{f} &= C_1\mathbf{g}^1(\mathbf{L}\cdot\mathbf{T})(\mathbf{L}\cdot\mathbf{N}) + C_2\mathbf{g}^2(\mathbf{M}\cdot\mathbf{T})(\mathbf{M}\cdot\mathbf{N}).\end{aligned} \tag{37}$$

which are expressions of edge tractions, edge moments and the corner forces, respectively. For example, if the fiber's directions are either normal or tangential to the boundary (i.e., $(\mathbf{L}\cdot\mathbf{T})(\mathbf{L}\cdot\mathbf{N}) = 0$ and $(\mathbf{M}\cdot\mathbf{T})(\mathbf{M}\cdot\mathbf{N}) = 0$), Eq. (37) further reduces to

$$\begin{aligned}t_i &= P_{iA}N_A,\\ m_i &= C_1 g_i^1 L_A N_A L_B N_B + C_2 g_i^2 M_A N_A M_B N_B,\\ f_i &= 0,\end{aligned} \tag{38}$$

where

$$\begin{aligned}P_{iA} &= \mu F_{iA} - pF_{iA}^* - C_1 g_{i,B}^1 L_A L_B - C_2 g_{i,B}^2 M_A M_B,\\ g_i^1 &= F_{iA,B}L_A L_B \text{ and } g_i^2 = F_{iA,B}M_A M_B.\end{aligned}$$

4 Linear theory

We consider superposed "*small*" deformations as

$$\chi = \chi_o + \varepsilon\dot{\chi}\ ; \quad |\varepsilon| \ll 1, \tag{39}$$

where $(*)_o$ denote configuration of $*$ evaluated at $\varepsilon = 0$ and $(\dot{*}) = \partial(*)/\partial\varepsilon$. In particular, we denote $\dot{\chi} = \mathbf{u}$. Here caution needs to be taken that the present notation is not confused with the one used for the variational computation. Details regarding the following developments can also be found in [46] where the authors discussed a compatible linear theory in a similar context. From Eq. (39), the deformation gradient tensor can be written by

$$\mathbf{F} = \mathbf{F}_o + \varepsilon\nabla\mathbf{u}, \ \text{where}\, \dot{\mathbf{F}} = \nabla\mathbf{u}. \tag{40}$$

We assume that the body is initially undeformed and stress free at $\varepsilon = 0$ (i.e., $\mathbf{F}_o = \mathbf{I}$ and $\mathbf{P}_o = \mathbf{0}$). Hence, Eq. (40) becomes

$$\mathbf{F} = \mathbf{I} + \varepsilon\nabla\mathbf{u}, \tag{41}$$

and successively obtain

$$\mathbf{F}^{-1} = \mathbf{I} - \varepsilon\nabla\mathbf{u} + o(\varepsilon), \tag{42}$$

and

$$J = \det\mathbf{F} = 1 + \varepsilon\,\mathrm{div}\,\mathbf{u} + o(\varepsilon). \tag{43}$$

Further, in view of Eq. (39), Eq. (20) can be rewritten as

$$\mathrm{Div}(\mathbf{P}) = \mathrm{Div}(\mathbf{P}_o) + \varepsilon\mathrm{Div}(\dot{\mathbf{P}}) + o(\varepsilon) = \mathbf{0}. \tag{44}$$

By dividing the above by ε and letting $\varepsilon \to 0$, we have

$$\mathrm{Div}(\dot{\mathbf{P}}) = 0, \tag{45}$$

which serves as the linearized Euler equation. Now, from Eq. (19), the induced variation of $\mathbf{P}$ with respect to ε is given by

$$\dot{\mathbf{P}} = W_{\mathbf{FF}}\dot{\mathbf{F}} - \dot{p}\mathbf{F}_o^* - p_o\dot{\mathbf{F}}^* - C_1\nabla\dot{\mathbf{g}}^1(\mathbf{L}\otimes\mathbf{L}) - C_2\nabla\dot{\mathbf{g}}^2(\mathbf{M}\otimes\mathbf{M}), \tag{46}$$

where, in the case of neo-Hookean material [Eq. (21)]; $W_{\mathbf{FF}} = \mu(\mathbf{e}_i\otimes\mathbf{E}_A\otimes\mathbf{e}_i\otimes\mathbf{E}_A)$. Thus, Eqs. (45–46) yield

$$\mathrm{Div}(\mu\dot{\mathbf{F}}) - \mathrm{Div}(\dot{p}\mathbf{F}_o^*) - \mathrm{Div}(p_o\dot{\mathbf{F}}^*) - \mathrm{Div}[C_1\nabla\dot{\mathbf{g}}^1(\mathbf{L}\otimes\mathbf{L}) + C_2\nabla\dot{\mathbf{g}}^2(\mathbf{M}\otimes\mathbf{M})] = 0. \tag{47}$$

However, from Eq. (39), the terms in the above further reduce to

$$\mathrm{Div}(\mu\dot{\mathbf{F}}) = \mathrm{Div}(\mu\nabla\mathbf{u}) = \mu u_{i,AA}\mathbf{e}_i, \tag{48}$$

$$\mathrm{Div}(\dot{p}\mathbf{F}_o^*) = \mathbf{F}_o^*\nabla\dot{p} = \mathbf{I}\nabla\dot{p}, \because \mathrm{Div}(\mathbf{F}^*) = 0, \tag{49}$$

where $\mathbf{I}\nabla\dot{p}$ is on the current basis (i.e., $\mathbf{I}\nabla\dot{p} = \dot{p}_{,i}\mathbf{e}_i$) and

$$\mathrm{Div}(p_o\dot{\mathbf{F}}^*) = p_o\mathrm{Div}(\dot{\mathbf{F}^*}) = 0\ , \ \because p_o = \mu = \text{constant}. \tag{50}$$

We mention here that $p_o = \mu$ to recover the initial stress free state at $\varepsilon = 0$ from the underlying finite deformation(i.e.,$\mathbf{P}_o = \mu\mathbf{F}_o - p\mathbf{F}_o^* - C_1\nabla\mathbf{g}_o^1(\mathbf{L}\otimes\mathbf{L}) - C_2\nabla\mathbf{g}_o^2(\mathbf{M}\otimes\mathbf{M}) = \mathbf{0}$). In addition, since $\nabla\mathbf{L} = \nabla\mathbf{M} = 0$ for initially straight fibers, we evaluate

$$\begin{aligned}
&\mathrm{Div}(C_1\nabla\dot{\mathbf{g}}^1(\mathbf{L}\otimes\mathbf{L}) + C_2\nabla\dot{\mathbf{g}}^2(\mathbf{M}\otimes\mathbf{M}))\\
&= C_1\mathrm{Div}[u_{i,ABCD}L_AL_BL_CL_D(\mathbf{e}_i\otimes\mathbf{E}_D)] + C_2\mathrm{Div}[u_{i,ABCD}M_AM_BM_CM_D(\mathbf{e}_i\otimes\mathbf{E}_D)]\\
&= C_1u_{i,ABCD}L_AL_BL_CL_D\mathbf{e}_i + C_2u_{i,ABCD}M_AM_BM_CM_D\mathbf{e}_i, \quad \because \dot{\mathbf{F}} = \nabla\mathbf{u}.
\end{aligned} \tag{51}$$

Consequently, from Eqs. (47–51), the linearized Euler equation can be derived as

$$\mu u_{i,AA} - \dot{p}_{,i} - C_1u_{i,ABCD}L_AL_BL_CL_D - C_2u_{i,ABCD}M_AM_BM_CM_D = 0, \tag{52}$$

Also, in view of Eqs. (40–41) and (43), the condition of bulk incompressibility reduces to

$$(J-1)^{\cdot} = \mathbf{F}_o^* \cdot \dot{\mathbf{F}} = \operatorname{div} \mathbf{u} = \mathbf{0}. \tag{53}$$

In the case of an orthonormal family of fibers (i.e., $\mathbf{L} = \mathbf{E}_1,\ L_1 = 1,\ L_2 = 0,\ \mathbf{M} = \mathbf{E}_2,\ M_1 = 0,\ M_2 = 1$), Eq. (52) becomes

$$\dot{p}_{,i} = \mu u_{i,AA} - C_1 u_{i,1111} - C_2 u_{i,2222} \text{ for } i, A = 1, 2 \tag{54}$$

which, together with Eq. (53), serves as a compatible linear model of Eq. (26) for small deformations superposed on large. Finally, the boundary conditions in Eq. (37) can be linearized similarly as in the above (e.g., $\mathbf{t} = \mathbf{t}_o + \varepsilon\dot{\mathbf{t}} + o(e)$ etc…)

$$\begin{aligned}
\dot{\mathbf{t}} &= \mathbf{P}\dot{N} - \frac{\mathrm{d}}{\mathrm{d}S}\left[C_1\dot{\mathbf{g}}^1(\mathbf{L}\cdot\mathbf{T})(\mathbf{L}\cdot\mathbf{N}) + C_2\dot{\mathbf{g}}^2(\mathbf{M}\cdot\mathbf{T})(\mathbf{M}\cdot\mathbf{N})\right], \\
\dot{\mathbf{m}} &= C_1\dot{\mathbf{g}}^1(\mathbf{L}\cdot\mathbf{N})^2 + C_2\dot{\mathbf{g}}^2(\mathbf{M}\cdot\mathbf{N})^2, \\
\dot{\mathbf{f}} &= C_1\mathbf{g}^1(\mathbf{L}\cdot\mathbf{T})(\mathbf{L}\cdot\mathbf{N}) + C_2\dot{\mathbf{g}}^2(\mathbf{M}\cdot\mathbf{T})(\mathbf{M}\cdot\mathbf{N}).
\end{aligned} \tag{55}$$

In particular, if the fiber's directions are either normal or tangential to the boundary (i.e., $(\mathbf{L}\cdot\mathbf{T})(\mathbf{L}\cdot\mathbf{N}) = 0$ and $(\mathbf{M}\cdot\mathbf{T})(\mathbf{M}\cdot\mathbf{N}) = 0$), Eq. (55) reduces to

$$\begin{aligned}
\dot{t}_i &= \dot{P}_{iA}N_A, \\
\dot{m}_i &= C_1\dot{g}_i^1 L_A N_A L_B N_B + C_2\dot{g}_i^2 M_A N_A M_B N_B, \\
\dot{f}_i &= 0,
\end{aligned} \tag{56}$$

where

$$\begin{aligned}
\dot{P}_{iA} &= \mu u_{i,A} - \dot{p}(F_{iA}^*)_o - p_o\dot{F}_{iA}^* - C_1 g_{i,B}^1 L_A L_B - C_2 g_{i,B}^2 M_A M_B, \\
\dot{g}_i^1 &= u_{i,AB}L_A L_B, \quad \dot{g}_i^2 = F_{iA,B}M_A M_B,
\end{aligned} \tag{57}$$

and

$$(F_{iA}^*)_o = \delta_{iA}, \quad \because (F_{iA})_o = \delta_{iA} \ \text{ at } \varepsilon = 0. \tag{58}$$

Further, since $J\partial F_{jB}^*/\partial F_{iA} = F_{jB}^*F_{iA}^* - F_{iB}^*F_{jA}^*$ at $\mathbf{F}_o = \mathbf{I}$, we obtain

$$(\partial F_{jB}^*/\partial F_{iA})_o = \delta_{jB}\delta_{iA} - \delta_{iB}\delta_{jA} \text{ and } (\mathbf{F}_{\mathbf{F}}^*[\dot{\mathbf{F}}])_{jB} = (\delta_{jB}\delta_{iA} - \delta_{iB}\delta_{jA})u_{i,A}. \tag{59}$$

Thus

$$\dot{F}_{iA}^* = (\mathrm{Div}\mathbf{u})\delta_{iA} - u_{A,i} = -u_{A,i}, \tag{60}$$

where $\mathrm{Div}\mathbf{u} = \operatorname{div}\mathbf{u} = 0$ from the Linearized incompressibility condition. We note that, in the superposed incremental deformations, there is no clear distinction between current and deformed configuration (i.e., $\mathbf{e}_\alpha = \mathbf{E}_\alpha$).

4.1 Solution to the linearized problem

We introduce scalar field ϕ as

$$\mathbf{u} = \mathbf{k}\times\nabla\phi,\ \mathbf{k}(\text{unit normal});\ u_i = \varepsilon_{\lambda i}\phi_{,\lambda}, \tag{61}$$

so that Eq. (53) can be automatically satisfied (i.e., $\phi_{,12} - \phi_{,21} = 0$). Thus, the linearized Euler equation [Eq. (54)] can be rewritten as

$$\dot{p}_{,i} = \mu\varepsilon_{\lambda i}(\phi_{,\lambda 11} + \phi_{,\lambda 22}) - C_1\varepsilon_{\lambda i}\phi_{,\lambda 1111} - C_2\varepsilon_{\lambda i}\phi_{,\lambda 2222}. \tag{62}$$

By utilizing the compatibility condition of $\dot{p}_{,i}$ (i.e., $\dot{p}_{,ij} = \dot{p}_{,ji}$), we obtain the following partial differential equation solving for ϕ.

$$(\phi_{,1111} + 2\phi_{,1122} + \phi_{,2222}) - \frac{C_1}{\mu}(\phi_{,11} + \phi_{,22})_{,1111} - \frac{C_2}{\mu}(\phi_{,11} + \phi_{,22})_{,2222} = 0. \tag{63}$$

It is worth mentioning here that the solution of Eq. (63) is not accommodated by the conventional methods such as the Fourier transform and the separation of variables. Instead, we adopt the methods of iterative reduction and principle of eigenfunction expansion and obtain the potential function for $\phi(x,\ y)$. The details which can be found in [35–37] are intentionally omitted for the sake of conciseness. The analytical solution ϕ is then converted through mapping $\chi = (X_1 - \phi_{,2})\mathbf{e}_1 + (X_2 + \phi_{,1})\mathbf{e}_2$ to obtain the complete deformed configurations (see Figs. 4, 5, 6, 7). Accordingly, the general solution of Eq. (63) can be found as

$$
\begin{aligned}
\phi = \sum_{m=1}^{\infty} \{ & e^{\frac{\sqrt{2m\sqrt{\alpha_1}+1}}{2\sqrt{\alpha_1}}x}\left(A_m\cos\left(\frac{\sqrt{2m\sqrt{\alpha_1}-1}}{2\sqrt{\alpha_1}}x\right)+B_m\sin\left(\frac{\sqrt{2m\sqrt{\alpha_1}-1}}{2\sqrt{\alpha_1}}x\right)\right)\\
& e^{-\frac{\sqrt{2m\sqrt{\alpha_1}+1}}{2\sqrt{\alpha_1}}x}\left(C_m\cos\left(\frac{\sqrt{2m\sqrt{\alpha_1}-1}}{2\sqrt{\alpha_1}}x\right)+D_m\sin\left(\frac{\sqrt{2m\sqrt{\alpha_1}-1}}{2\sqrt{\alpha_1}}x\right)\right)\}\\
& \times\left\{E_m\ \cosh\left(\frac{\sqrt{1+\sqrt{4\alpha_2m^2+1}}}{\sqrt{2\alpha_2}}y\right)+F_m\sinh\left(\frac{\sqrt{1+\sqrt{4\alpha_2m^2+1}}}{\sqrt{2\alpha_2}}y\right)\right.\\
& \left.+G_m\cos\left(\frac{\sqrt{\sqrt{4\alpha_2m^2+1}-1}}{\sqrt{2\alpha_2}}y\right)+H_m\sin\left(\frac{\sqrt{\sqrt{4\alpha_2m^2+1}-1}}{\sqrt{2\alpha_2}}y\right)\right\}\\
& +\sum_{n=1}^{\infty}\left\{e^{\frac{\sqrt{2n\sqrt{\alpha_2}+1}}{2\sqrt{\alpha_2}}x}\left(A_n\cos\left(\frac{\sqrt{2n\sqrt{\alpha_2}-1}}{2\sqrt{\alpha_2}}y\right)+B_n\sin\left(\frac{\sqrt{2n\sqrt{\alpha_2}-1}}{2\sqrt{\alpha_2}}y\right)\right)\right.\\
& \left.e^{-\frac{\sqrt{2n\sqrt{\alpha_2}+1}}{2\sqrt{\alpha_2}}x}\left(C_n\cos\left(\frac{\sqrt{2n\sqrt{\alpha_2}-1}}{2\sqrt{\alpha_2}}y\right)+D_n\sin\left(\frac{\sqrt{2n\sqrt{\alpha_2}-1}}{2\sqrt{\alpha_2}}y\right)\right)\right\}\\
& \times\left\{E_n\ \cosh\left(\frac{\sqrt{1+\sqrt{4\alpha_1n^2+1}}}{\sqrt{2\alpha_1}}x\right)+F_n\sinh\left(\frac{\sqrt{1+\sqrt{4\alpha_1n^2+1}}}{\sqrt{2\alpha_1}}x\right)\right.\\
& \left.+G_n\cos\left(\frac{\sqrt{\sqrt{4\alpha_1n^2+1}-1}}{\sqrt{2\alpha_1}}x\right)+H_n\sin\left(\frac{\sqrt{\sqrt{4\alpha_1n^2+1}-1}}{\sqrt{2\alpha_1}}x\right)\right\},
\end{aligned}
\tag{64}
$$

where $\alpha_1 = C_1/\mu$ and $\alpha_2 = C_2/\mu$. The unknown constant real numbers A_m, B_m, C_m, D_m, E_m, F_m, G_m, H_m, A_n, B_n, C_n, D_n, E_n, F_n, G_n and H_n can be completely determined by imposing admissible boundary conditions as depicted in Eqs. (56–60). The corresponding stress fields can also be obtained through Eqs. (57) and (61–62). For example, in the case of symmetric bending (see Fig. 1), where

$$
\begin{aligned}
&\dot{\mathbf{m}} = \dot{m}_1\mathbf{e}_1 + \dot{m}_2\mathbf{e}_2,\ \ \dot{m}_1 = C_1u_{1,11} = -\phi_{,211} = 5 \approxeq \sum_{n=1}^{30}\frac{20}{\pi n}(-1)^{\frac{n-1}{2}}\cos\left(\frac{\pi n}{2d}\right)y\mathbf{e}_m,\\
&\dot{m}_2 = 0,
\end{aligned}
\tag{65}
$$

and for top and bottom surfaces, we impose

$$
\begin{aligned}
&\dot{\mathbf{m}} = \dot{m}_1\mathbf{e}_1 + \dot{m}_2\mathbf{e}_2,\ \ \dot{m}_2 = C_2u_{2,22} = \phi_{,122} = 0.001 = \sum_{m=1}^{30}\frac{0.004}{\pi m}(-1)^{\frac{m-1}{2}}\cos\left(\frac{\pi m}{2c}\right)x,\\
&\dot{m}_1 = 0.
\end{aligned}
\tag{66}
$$

The applied moment is approximated using Fourier series [see Eqs. (65–66)] indicating fast convergence (within 30 iterations) and the corresponding results are summarized through Figs. 4, 5, 6 and 7. Despite the inherent complexities of the present PDE (e.g., non-smooth/singular behavior of the potential as approaching a boundary, discontinuities on the corner vertices), the solution is smooth and stable throughout the entire domain of interest and displays good agreement with both the experiments [33] and the corresponding numerical results for a "*small*" deformation regime (see, Figs. 4, 5, 6, 7, 9, 10, 11).

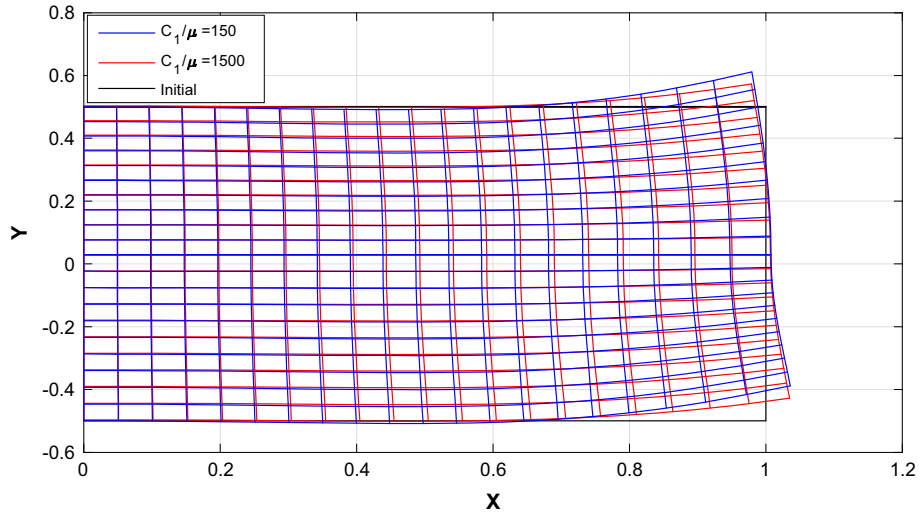

Fig. 4 Deformed configurations with respect to C_1/μ when $M/\mu = 50$ and $C_2/\mu = 100$

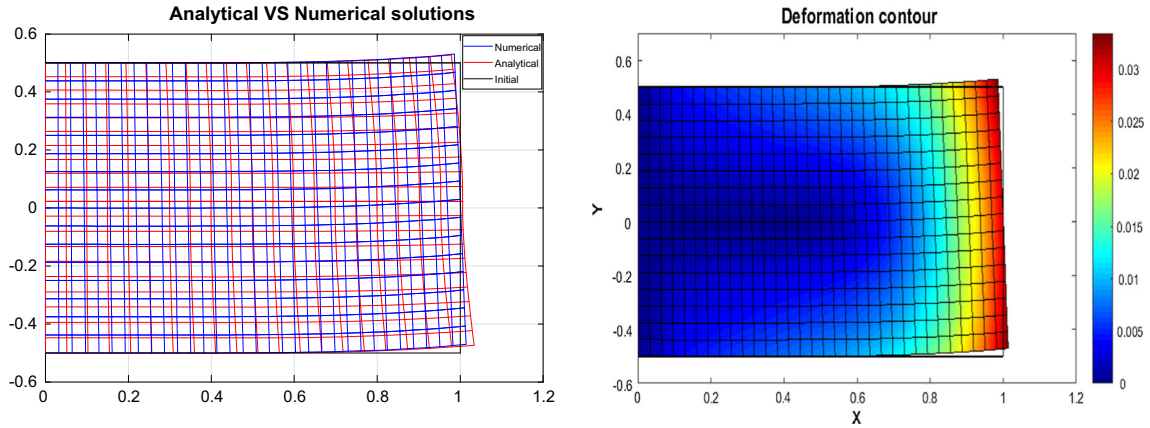

Fig. 5 Deformed configurations when $\frac{C_1}{\mu} = 150$, $\frac{C_2}{\mu} = 100$, $\frac{M}{\mu} = 10$

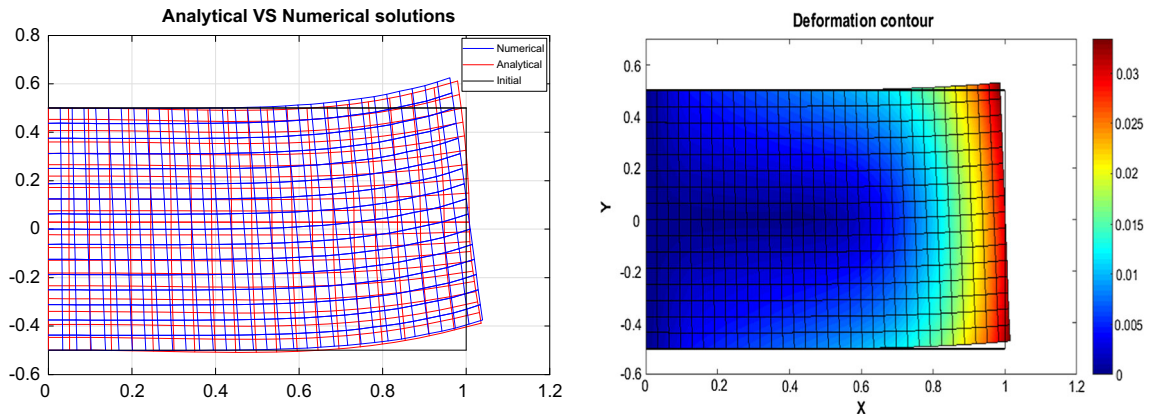

Fig. 6 Deformed configurations when $\frac{C_1}{\mu} = 150$, $\frac{C_2}{\mu} = 100$, $\frac{M}{\mu} = 30$

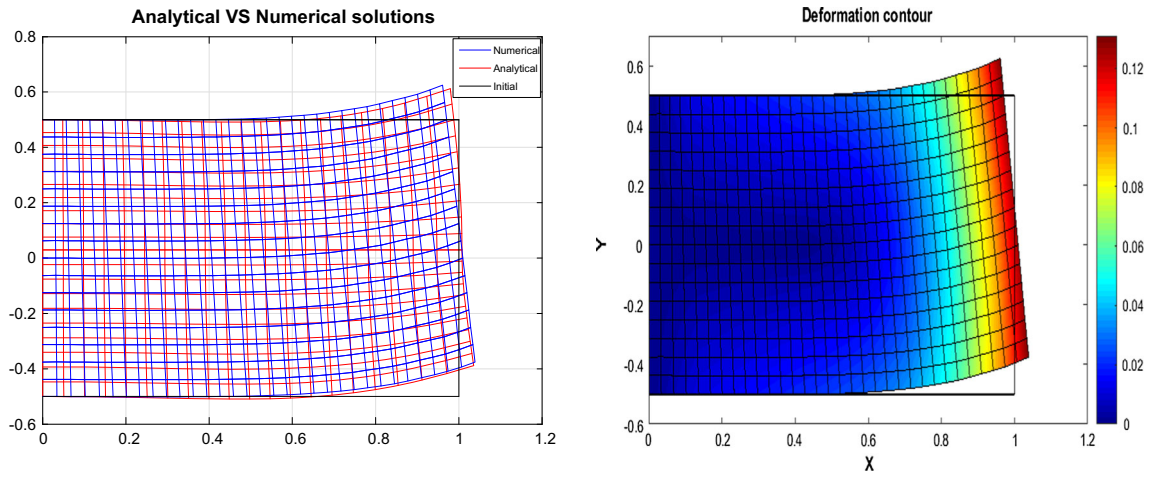

Fig. 7 Deformed configurations when $\frac{C_1}{\mu} = 150$, $\frac{C_2}{\mu} = 100$, $\frac{M}{\mu} = 50$

Table 1 Maximum deflections: experimental results versus theoretical predictions

$\text{Load}_{\text{applied}}$ (N)	Experiment (mm)	Theory (mm)
0.1	0.349	0.339
0.2	0.682	0.667
0.3	1.001	1.001
0.4	1.329	1.335
0.5	1.659	1.669
0.6	2.002	2.003
0.7	2.380	2.336

5 Model verification and validation via experimental results

A comparison with experimental results is performed in this section to determine the accuracy and utility of the proposed model. Two sets of experiments are considered for the purpose: one from the inhouse experimental setting and the other from the work of [33].

5.1 Three-point bending test: CNC fiber composite

In the experiment, a composite reinforced with crystalline nanocellulose (CNC) fibers ($C_1 = 150\,\text{GPa}$, $\mu = 1\,\text{GPa}$) is placed on three-point bending (at -10, 0, and 10 mm) and the out of plane direction (x_3) is aligned with the loading cylinder (see, Fig. 8). The applied loads and resulting displacements are simultaneously recorded via the MTS road cell and data logger. This setting is a special case of the proposed model when $c \gg d$ and $C_1/\mu = 150$ with vanishing C_2/μ (see, Fig. 1). The obtained solution successfully predicts the normal deflections of the CNC composite strip with a configuration factor $\gamma = 0.526[L]^2$ between the applied load and input stress on each simulation (i.e., $\sigma_{\text{input}} \times \gamma = \text{Load}_{\text{applied}}$; see, Table 1). Detailed discussions regarding the second-gradient theory and it's applications in the relevant experiments can be found in [47–49]. In addition, using a commercial image processing tool, the experimental deformed profiles are also obtained (maximum deflections at 2.55 and 3 mm) and compared with the theoretical predictions. The resulting deformation profiles from both the experiments and theoretical simulations demonstrate a close correspondence throughout the domain of interest (see, Fig. 9).

5.2 Bending test of bidirectional fiber composites

With regard to the bending test of bidirectional fiber composite reinforced with E glass and T700S carbon fibers, we took the experimental results from the work of Dong and Davies ([33]; Fig. 2 and Table 2). Three

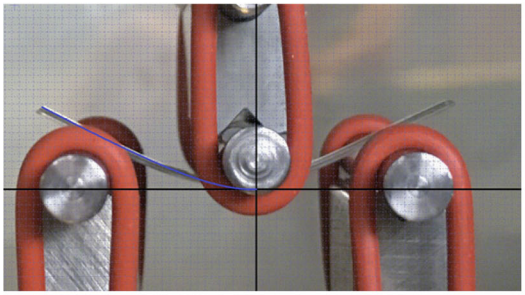

Maximum deflection $2.55mm$

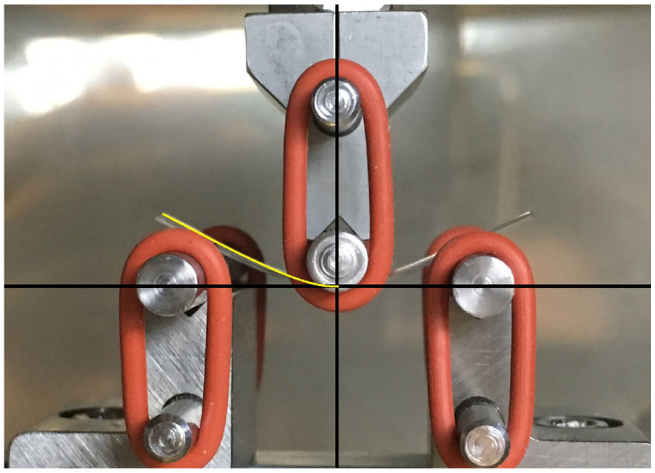

Maximum deflection $3mm$

Fig. 8 Experimental setting and image processing (2.55 and 3 mm): CNC fiber composite

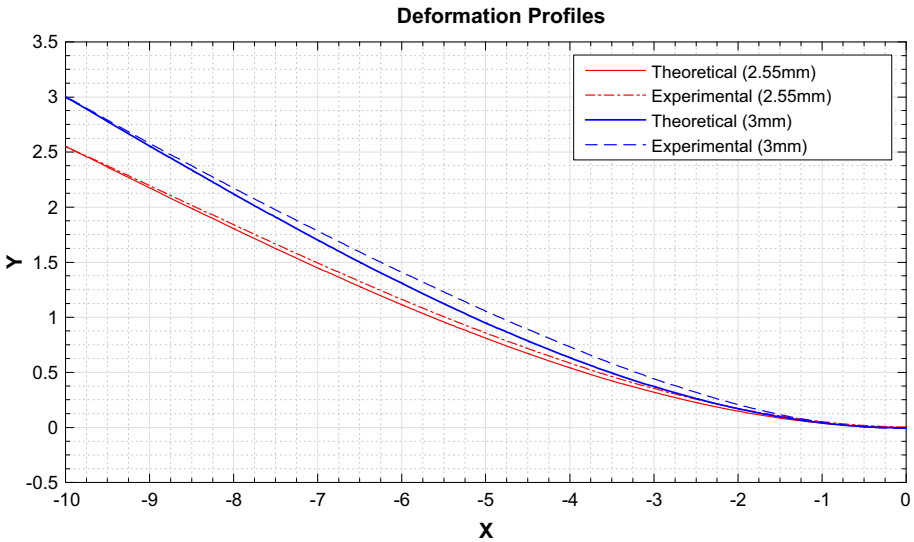

Fig. 9 Deformation profiles: theoretical predictions versus experimental results

experimental samples are considered: carbon–carbon fiber; carbon–glass fiber; and glass–glass fiber composites with fiber's volume fraction 37.2, 32.9 and 30.9%, respectively. These fibers are mounted in the matrix material in the same manner as illustrated in Fig. 1. In each simulation, the material properties of carbon and glass fibers are accommodated by the parameters C_1 and C_2 (e.g., C_1 = carbon = 4900 MPa, C_2 = glass = 2240 MPa for a carbon–glass fiber composite etc…). The carbon–glass fiber composite case with volume fraction 32.9% is used for benchmarking data in the identification of the configuration factor $\gamma = 0.936$ (see, Fig. 10). The factor is then uniformly applied for the other simulations, with the effects of different fibers' volume fractions taken into account. It is clear from Figs. 10–12 that predictions from both the nonlinear (numerical) and linear (analytical) theory demonstrate a close agreement with the experimental data. In addition, the proposed model assimilates the results presented in [26] which demonstrates good agreement up to linear regime (see, Fig. 13). These, in turn, suggest that the second gradient of the deformations, incorporated in the present model, accurately represents fiber's resistant to flexure. Overall, the proposed models perform well in the prediction of the mechanical behavior of fiber-reinforced composites and therefore they can be easily adopted in field exercises. In particular, the one from the linear theory is more useful, as it provides an explicit form of solution rather than a discretized solution.

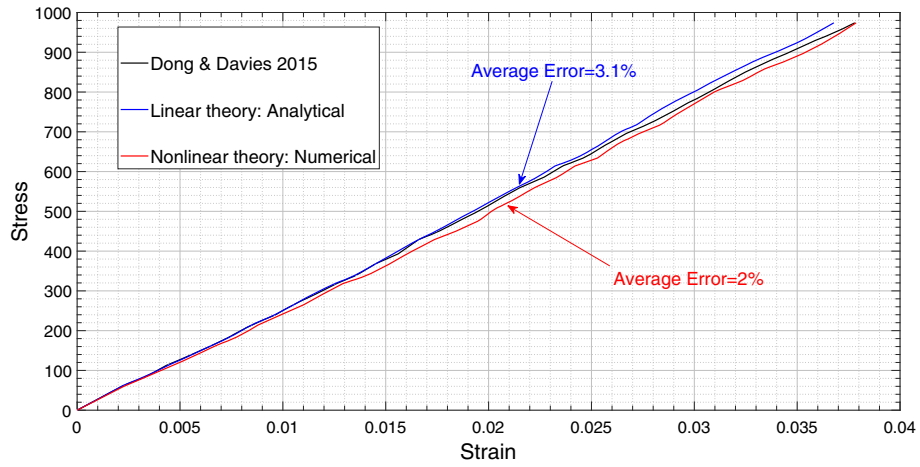

Fig. 10 Strain–stress curve (carbon–glass fiber composite) :Reproduced with permission from Dong and Davies [33]

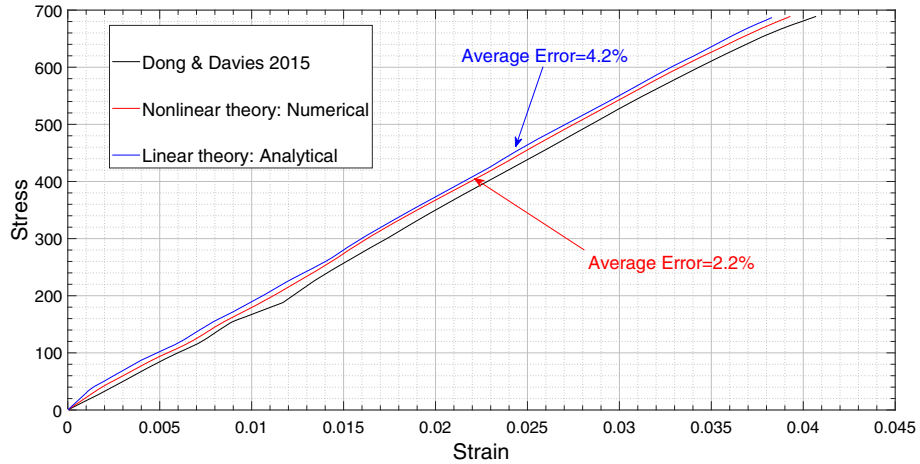

Fig. 11 Strain–stress curve (glass–glass fiber composite) :Reproduced with permission from Dong and Davies [33]

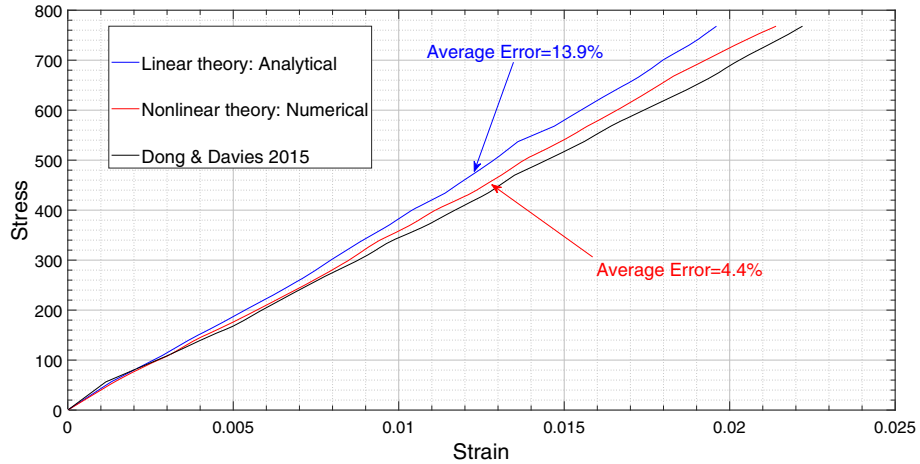

Fig. 12 Strain–stress curve (carbon–carbon fiber composite) :Reproduced with permission from Dong and Davies [33]

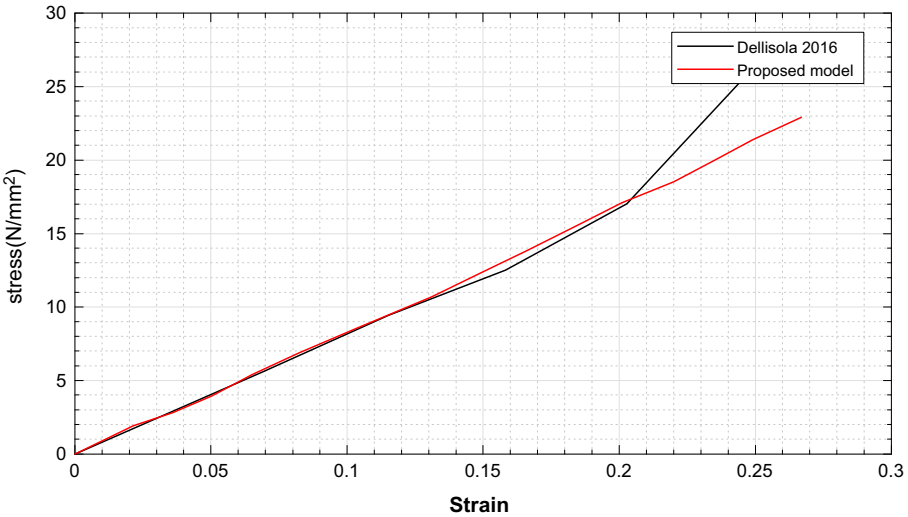

Fig. 13 Strain–stress curve: proposed model versus dell'Isola 2016

6 Conclusion

In this study, a continuum-based model for the mechanics of an elastic solid reinforced with bidirectional fibers is presented in finite plane elastostatics. Throughout the computation of variational derivatives along the arc length of fibers and the virtual–work statement, the Euler equilibrium equation is obtained within which the constraint of bulk incompressibility is augmented. A complete derivation of the admissible boundary conditions is also discussed for the sake of clarity. In addition, an implementation of the proposed model is made in the case of neo-Hookean materials reinforced with bidirectional fibers and undergoing finite plane deformations. The obtained solution from the resulting PDEs successfully predicts both the deformed configurations of the CNC composite subjected to flexural loads, and the evaluations of the effective moduli of T700S carbon–E glass fiber composite.

In particular, within the setting of superposed incremental deformations, a complete linear theory is developed including the rigorous derivations of the corresponding Euler equation, admissible boundary conditions and constraint of bulk incompressibility. The resulting equation is solved analytically, leading to a comprehensive description of the mechanics of a bidirectional composite subjected to flexural loads. More importantly, the solution demonstrates a close correspondence with both the experimental results and numerical simulations within small deformations and displays smooth and stable behavior throughout the elastic solid. Lastly, we mention that the case of fiber extensibility is intentionally excluded from the analysis which can be easily accounted for via the modification of the proposed energy density function.

Acknowledgements This work was supported by the Natural Sciences and Engineering Research Council of Canada via Grant #RGPIN 04742 and the University of Alberta through a start-up grant. Kim would like to thank Dr. David Steigmann for discussions concerning the underlying theory. Kim would also like to thank Dr. Cagri Ayranci and Ms. Irina Garance for the experimental data.

Appendix: Finite element analysis of the fourth-order coupled PDE

It is not trivial to demonstrate numerical analysis procedures for coupled PDE systems, especially for those with high-order terms due to the C^1 continuity of the corresponding Hilbert space. For preprocessing, Eq. (26) can be recast as

$$
\begin{aligned}
&\mu\,(R+F) - A\chi_{2,2} + B\chi_{2,1} - C_1 R_{,11} - C_2 F_{,22} = 0,\\
&\mu\,(Q+G) + A\chi_{1,2} - B\chi_{1,1} - C_1 Q_{,11} - C_2 G_{,22} = 0,\\
&C\chi_{2,2} - D\chi_{1,2} - 1 = 0, \quad Q - \chi_{1,11} = 0,\\
&R - \chi_{2,11} = 0, \quad C - \chi_{1,1} = 0, \quad D - \chi_{2,1} = 0,
\end{aligned}
$$

$$
\begin{aligned}
&F-\chi_{1,22}=0,\quad G-\chi_{2,22}=0,\\
&A-\mu(\chi_{1,11}+\chi_{1,22})-C_1R_{,11}-C_2F_{,22}=0,\\
&B-\mu(\chi_{2,11}+\chi_{2,22})-C_1Q_{,11}-C_2G_{,22}=0.
\end{aligned}
\tag{67}
$$

where $Q=\chi_{1,11}$, $R=\chi_{2,11}$, $F=\chi_{1,22}$, $G=\chi_{2,22}$, $C=\chi_{1,1}$ and $D=\chi_{2,1}$. The nonlinear terms in the above can be treated as

$$
\begin{aligned}
-A\chi_{2,2}+B\chi_{2,1} &\Longrightarrow -A_0\chi_{2,2}+B_0\chi_{2,1},\\
A\chi_{1,2}-B\chi_{1,1} &\Longrightarrow A_0\chi_{1,2}-B_0\chi_{1,1},\\
C\chi_{2,2}-D\chi_{2,1} &\Longrightarrow C_0\chi_{2,2}-D_0\chi_{2,1},
\end{aligned}
\tag{68}
$$

where the values of A, B and C continue to be refreshed based on their previous estimations (A_0, B_0, C_0) as iteration progresses. Therefore, the weak form of Eq. (67) is obtained by

$$
\begin{aligned}
0=&\int_{\Omega}(\mu w_1R-\mu w_1F-w_1A_0\chi_{2,2}+w_1B_0\chi_{2,1}+C_1w_{1,1}R_{,1}+C_2w_{1,2}F_{,2})\mathrm{d}\Omega\\
&-\int_{\partial\Gamma}(C_1w_1R_{,1}+C_2w_1F_{,2})N\mathrm{d}\Gamma,\\
0=&\int_{\Omega}(\mu w_2Q-\mu w_2G+w_2A_0\chi_{1,2}-w_2B_0\chi_{1,1}+C_1w_{2,1}Q_{,1}+C_2w_{2,2}G_{,2})\mathrm{d}\Omega\\
&-\int_{\partial\Gamma}(C_1w_2Q_{,1}+C_2w_2G_{,2})N\mathrm{d}\Gamma,\\
0=&\int_{\Omega}C_0w_3\chi_{2,2}-D_0w_3\chi_{1,2}-w_3)\mathrm{d}\Omega,\ 0=\int_{\Omega}(w_4Q+w_{4,1}\chi_{1,1})\mathrm{d}\Omega-\int_{\partial\Gamma}(w_4\chi_{1,1})N\mathrm{d}\Gamma,\\
0=&\int_{\Omega}(w_5R+w_{5,1}\chi_{2,1})\mathrm{d}\Omega-\int_{\partial\Gamma}(w_5\chi_{2,1})N\mathrm{d}\Gamma,\ 0=\int_{\Omega}(w_6C-w_6\chi_{1,1})\mathrm{d}\Omega,\\
0=&\int_{\Omega}(w_7D-w_7\chi_{2,1})\mathrm{d}\Omega,\ 0=\int_{\Omega}(w_8F+w_{8,2}\chi_{1,2})\mathrm{d}\Omega-\int_{\partial\Gamma}(w_8\chi_{1,2})N\mathrm{d}\Gamma,\\
0=&\int_{\Omega}(w_9G+w_{9,2}\chi_{2,2})\mathrm{d}\Omega-\int_{\partial\Gamma}(w_9\chi_{2,2})N\mathrm{d}\Gamma,\\
0=&\int_{\Omega}(w_{10}A+\mu w_{10,1}\chi_{1,1}-\mu w_{10,2}\chi_{1,2}+C_1w_{10,1}R_{,1})\mathrm{d}\Omega-\int_{\partial\Gamma}(\mu w_{10}\chi_{1,1})N\mathrm{d}\Gamma+\\
&\int_{\partial\Gamma}(\mu w_{10}\chi_{1,2})N\mathrm{d}\Gamma-\int_{\partial\Gamma}(C_1w_{10}R_{,1}+C_2w_{10}F_{,2})N\mathrm{d}\Gamma,\\
0=&\int_{\Omega}(w_{11}B+\mu w_{11,1}\chi_{2,1}-\mu w_{11,2}\chi_{2,2}+C_1w_{11,1}Q_{,1})\mathrm{d}\Omega-\int_{\partial\Gamma}(\mu w_{11}\chi_{2,1})N\mathrm{d}\Gamma+\\
&\int_{\partial\Gamma}(\mu w_{11}\chi_{2,2})N\mathrm{d}\Gamma-\int_{\partial\Gamma}(C_1w_{11}Q_{,1}+C_2w_{11}G_{,2})N\mathrm{d}\Gamma,
\end{aligned}
\tag{69}
$$

where the unknowns (e.g., χ_1, χ_2, Q_1, R_1, A, B etc.) can be written in the form of Lagrangian polynomial such that $(*)=\sum_{j=1}^{n}[(*)_j\Psi_j(x,y)]$. Ω, $\partial\Gamma$ and $\mathbf{N}$ are the domain of interest, the associated boundary, and the rightward unit normal to the boundary $\partial\Gamma$ in the sense of the Green–Stoke's theorem, respectively. The corresponding test function w is given by

$$
w=\sum_{i=1}^{n}w_i\Psi_i(x,y),
\tag{70}
$$

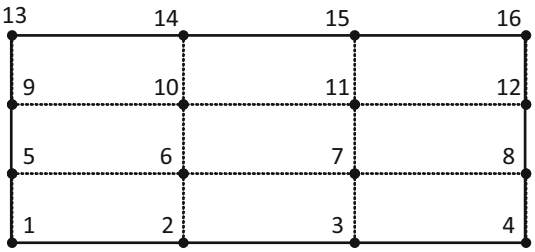

Fig. 14 Schematic of 16 nodes rectangular element

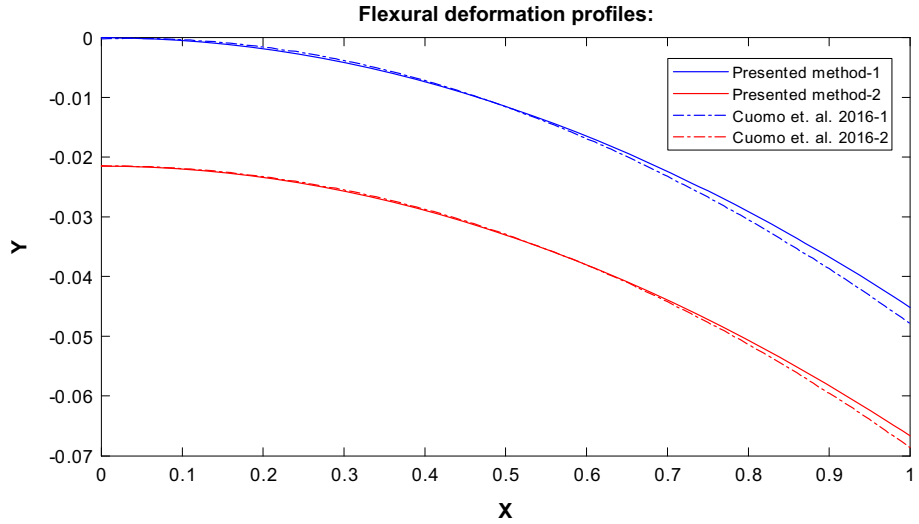

Fig. 15 Performance comparison: proposed method versus Cuomo et al. [22]

where w_i is weight of the test function and $\Psi_i(x, y)$ are the shape functions that

$$\begin{bmatrix} \psi_1 & \psi_5 & \psi_9 & \psi_{13} \\ \psi_2 & \psi_6 & \psi_{10} & \psi_{14} \\ \psi_3 & \psi_7 & \psi_{11} & \psi_{15} \\ \psi_4 & \psi_8 & \psi_{12} & \psi_{16} \end{bmatrix} = \begin{bmatrix} f_1 \\ f_2 \\ f_3 \\ f_4 \end{bmatrix} [\, g_1 \quad g_2 \quad g_3 \quad g_4 \,], \tag{71}$$

where

$$f_1(x) = \frac{\left(x - \frac{c}{3}\right)\left(x - \frac{2c}{3}\right)(x - c)}{\left(-\frac{c}{3}\right)\left(-\frac{2c}{3}\right)(-c)}, \quad f_2(x) = \frac{(x)\left(x - \frac{2c}{3}\right)(x - c)}{\left(\frac{c}{3}\right)\left(-\frac{c}{3}\right)\left(-\frac{2c}{3}\right)},$$
$$f_3(x) = \frac{(x)\left(x - \frac{c}{3}\right)(x - c)}{\left(\frac{2c}{3}\right)\left(\frac{c}{3}\right)\left(-\frac{c}{3}\right)}, \quad f_4(x) = \frac{(x)\left(x - \frac{c}{3}\right)\left(x - \frac{2c}{3}\right)}{\left(\frac{c}{3}\right)\left(\frac{2c}{3}\right)(c)}$$
$$g_1(y) = \frac{\left(y - \frac{d}{3}\right)\left(y - \frac{2d}{3}\right)(y - d)}{\left(-\frac{d}{3}\right)\left(-\frac{2d}{3}\right)(-d)}, \quad g_2(y) = \frac{(y)\left(y - \frac{2d}{3}\right)(y - d)}{\left(\frac{d}{3}\right)\left(-\frac{d}{3}\right)\left(-\frac{2d}{3}\right)},$$
$$g_3(y) = \frac{(y)\left(y - \frac{d}{3}\right)(y - d)}{\left(\frac{2d}{3}\right)\left(\frac{d}{3}\right)\left(-\frac{d}{3}\right)}, \quad g_4(y) = \frac{(y)\left(y - \frac{d}{3}\right)\left(y - \frac{2d}{3}\right)}{\left(\frac{d}{3}\right)\left(\frac{2d}{3}\right)(d)}.$$

The assignment of each shape function is illustrated in Fig. 14.

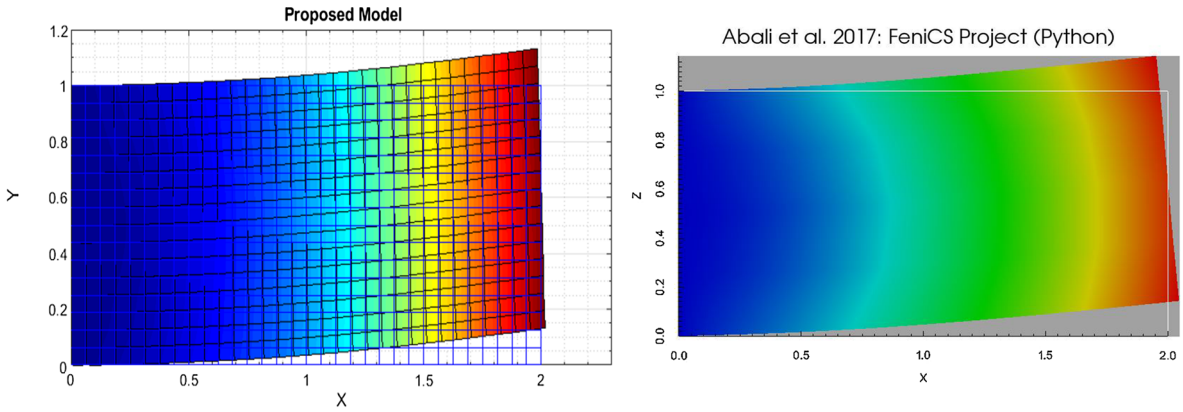

Fig. 16 Deformation contours: proposed method versus Abali et al. [50]

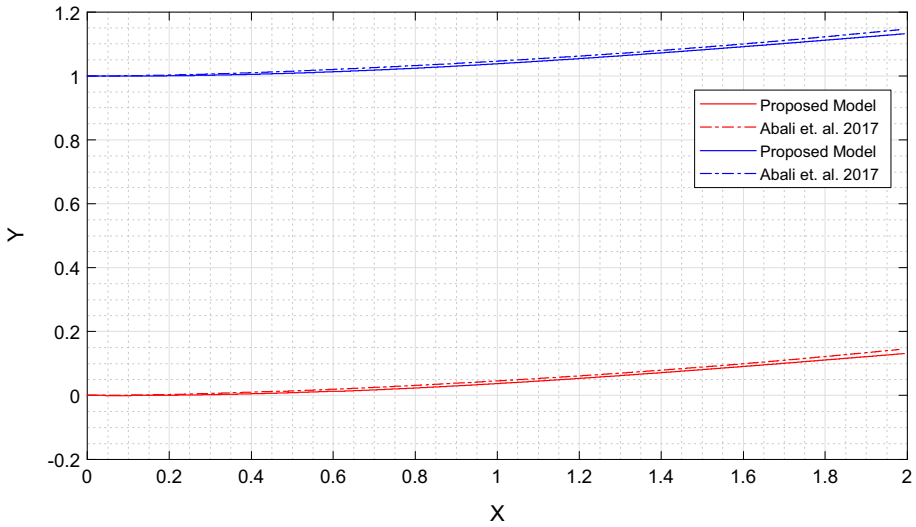

Fig. 17 Deformation profiles: proposed method versus Abali et al. [50]

Using Lagrangian polynomial representation, the first of Eq. (69) can be rewritten as

$$0 = \sum_{i,\ j=1}^{n} \left\{ \int_{\Omega} (\mu \Psi_i \Psi_j + C_1 \Psi_{i,1} \Psi_{j,1}) \mathrm{d}\Omega \right\} R_j + \sum_{i,\ j=1}^{n} \left\{ \int_{\Omega} (\mu \Psi_i \Psi_j + C_2 \Psi_{i,2} \Psi_{j,2}) \mathrm{d}\Omega \right\} F_j$$
$$- \sum_{i,\ j=1}^{n} \left\{ \int_{\Omega} (\Psi_i A_0 \Psi_{j,2} + \Psi_i B_0 \Psi_{j,1}) \mathrm{d}\Omega \right\} \chi_{2j} - \int_{\partial \Gamma} (C_1 \Psi_i R_{,1} + C_2 \Psi_i F_{,2}) N \mathrm{d}\Gamma. \tag{72}$$

and similarly for the rest of equations. Finally, we obtain the systems of equations $[\mathbb{K}][\mathbb{E}] = [\mathbb{F}]$. Here $[\mathbb{K}]$ and $[\mathbb{F}]$ are $[11 \times 10]$ and $[10 \times 1]$ matrices, respectively, and $[\mathbb{E}]$ is $[11 \times 1]$ matrix with unknowns (e.g., $\chi_1, \chi_2, Q_1, R_1, A, B$ etc.). The expressions of $\left[K^{ij}\right]$ and $[F_i]$ can be obtained via the standard finite element analysis procedures. For example,

$$K^{11} = \int_{\Omega} (\mu \Psi_i \Psi_j + C_2 \Psi_{i,2} \Psi_{j,2}) \mathrm{d}\Omega,$$

and

$$F_1 = \int_{\partial \Gamma} (C_1 \Psi_i R_{,1} + C_2 \Psi_i F_{,2}) N \mathrm{d}\Gamma.$$

Fig. 18 Convergence analysis

We mention here that other numerical scheme may be adopted such as the methods presented in [50,51]. Figure 15 illustrates performance comparison between the presented method and the one adopted in [51] which shows good agreement over the domain of interest. The deformation profiles and contours in Figs. 16 and 17 are the predictions from both the proposed numerical scheme and the method in [50,52,53]. Again, they produce almost identical predictions when performed in the analogous settings. Lastly, the presented numerical scheme demonstrates fast convergence within 70 iterations (see, Fig. 18).

References

1. Spencer, A.J.M.: Deformations of Fibre-Reinforced Materials. Oxford University Press, Oxford (1972)
2. Pipkin, A.C.: Stress analysis for fiber-reinforced materials. Adv. Appl. Mech. **19**, 1–51 (1979)
3. Boutin, C.: Microstructural effects in elastic composites. Int. J. Solids and Struct. **33**(7), 1023–1051 (1996)
4. Forest, S.: Homogenization methods and the mechanics of generalised continua part 2. Theor. Appl. Mech. **28**, 113–143 (2002)
5. Mulhern, J.F., Rogers, T.G., Spencer, A.J.M.: A continuum theory of a plastic–elastic fibre-reinforced material. Int. J. Eng. Sci. **7**, 129–152 (1969)
6. Pipkin, A.C., Rogers, T.G.: Plane deformations of incompressible fiber-reinforced materials. ASME J. Appl. Mech. **38**(8), 634–640 (1971)
7. Spencer, A.J.M., Soldatos, K.P.: Finite deformations of fibre-reinforced elastic solids with fibre bending stiffness. Int. J. Non-Linear Mech. **42**, 355–368 (2007)
8. Toupin, R.A.: Theories of elasticity with couple stress. Arch. Ration. Mech. Anal. **17**, 85–112 (1964)
9. Mindlin, R.D., Tiersten, H.F.: Effects of couple-stresses in linear elasticity. Arch. Ration. Mech. Anal. **11**, 415–448 (1962)
10. Koiter, W.T.: Couple-stresses in the theory of elasticity. Proc. K. Ned. Akad. Wetensc. B **67**, 17–44 (1964)
11. Park, H.C., Lakes, R.S.: Torsion of a micropolar elastic prism of square cross section. Int. J. Solids Struct. **23**, 485–503 (1987)
12. Maugin, G.A., Metrikine, A.V. (eds.): Mechanics of Generalized Continua: One Hundred Years After the Cosserats. Springer, New York (2010)
13. Neff, P.: A finite-strain elastic–plastic Cosserat theory for polycrystals with grain rotations. Int. J. Eng. Sci. **44**, 574–594 (2006)
14. Munch, I., Neff, P., Wagner, W.: Transversely isotropic material: nonlinear Cosserat vs. classical approach. Cont. Mech. Therm. **23**, 27–34 (2011)
15. Neff, P.: Existence of minimizers for a finite-strain micro-morphic elastic solid. Proc. R. Soc. Edinb. A **136**, 997–1012 (2006)
16. Park, S.K., Gao, X.L.: Variational formulation of a modified couple-stress theory and its application to a simple shear problem. Z. Angew. Math. Phys. **59**, 904–917 (2008)
17. Fried, E., Gurtin, M.E.: Gradient nanoscale polycrystalline elasticity: intergrain interactions and triple-junction conditions. J. Mech. Phys. Solids **57**, 1749–1779 (2009)
18. Steigmann, D.J.: Theory of elastic solids reinforced with fibers resistant to extension, flexure and twist. Int. J. Non-Linear Mech. **47**, 734–742 (2012)
19. Steigmann, D.J., dell'Isola, F.: Mechanical response of fabric sheets to three-dimensional bending, twisting, and stretching. Acta Mech. Sin. **31**(3), 373–382 (2015)

20. Placidi, L., Greco, L., Bucci, S., Turco, E., Rizzi, N.L.: A second gradient formulation for a 2D fabric sheet with inextensible fibres. Z. Angw. Math. Phys. **67**(5), 114 (2016)
21. Placidi, L., Barchiesi, E., Turco, E., Rizzi, N.L.: A review on 2D models for the description of pantographic fabrics. Z. Angw. Math. Phys. **67**(5), 121 (2016)
22. Cuomo, M., dell'Isola, F., Greco, L., Rizzi, N.L.: First versus second gradient energies for planar sheets with two families of inextensible fibres: investigation on deformation boundary layers, discontinuities and geometrical instabilities. Compos. Part B Eng. **115**, 423–448 (2017). https://doi.org/10.1016/j.compositesb.2016.08.043
23. dell'Isola, F., Cuomo, M., Greco, L., Della Corte, A.: Bias extension test for pantographic sheets: numerical simulations based on second gradient shear energies. J. Eng. Math. **103**(1), 127–157 (2017). https://doi.org/10.1007/s10665-016-9865-7
24. dell'Isola, F., Della Corte, A., Greco, L., Luongo, A.: Plane bias extension test for a continuum with two inextensible families of fibers: a variational treatment with Lagrange multipliers and a perturbation solution. Int. J. Solids Struct. **81**, 1–12 (2016)
25. dell'Isola, F., Lekszycki, T., Pawlikowski, M., Grygoruk, R., Greco, L.: Designing a light fabric metamaterial being highly macroscopically tough under directional extension: first experimental evidence. Z. Angw. Math. Phys. ZAMP **66**(6), 3473–3498 (2015)
26. dell'Isola, F., Giorgio, I., Pawlikowski, M., Rizzi, N.L.: Large deformations of planar extensible beams and pantographic lattices: heuristic homogenization, experimental and numerical examples of equilibrium. Proc. R. Soc. Lond. A **472**(2185), 20150790 (2016)
27. Zeidi, M., Kim, C.: Mechanics of fiber composites with fibers resistant to extension and flexure. Math. Mech. Solids (2017). https://doi.org/10.7939/R3Z892V17
28. Zeidi, M., Kim, C.: Finite plane deformations of elastic solids reinforced with fibers resistant to flexure: complete solution. Arch. Appl. Mech. (2017). https://doi.org/10.1007/s00419-018-1344-3
29. Landau, L.D., Lifshitz, E.M.: Theory of Elasticity, 3rd edn. Pergamon, Oxford (1986)
30. Dill, E.H.: Kirchhoff's theory of rods. Arch. Hist. Exact Sci. **44**, 1–23 (1992)
31. Antman, S.S.: Nonlinear Problems of Elasticity. Springer, Berlin (2005)
32. Dell'Isola, F., Steigmann, D.J.: A two-dimensional gradient-elasticity theory for woven fabrics. J. Elast. **118**(1), 113–125 (2015)
33. Dong, C., Davies, I.J.: Flexural strength of bidirectional hybrid epoxy composites reinforced by E glass and T700S carbon fibres. Compos. Part B **72**, 65–71 (2015)
34. Ogden, R.W.: Non-linear Elastic Deformations. Ellis Horwood Ltd., Chichester (1984)
35. Read, W.W.: Analytical solutions for a Helmholtz equation with Dirichlet boundary conditions and arbitrary boundaries. Math. Comput. Model. **24**(2), 23–34 (1996)
36. Read, W.W.: Series solutions for Laplace's equation with nonhomogeneous mixed boundary conditions and irregular boundaries. Math. Comput. Model. **17**(12), 9–19 (1993)
37. Huang, Y., Zhang, X.: General analytical solution of transverse vibration for orthotropic rectangular thin plates. J. Mar. Sci. Appl. **1**(2), 78–82 (2002)
38. Truesdell, C., Noll, W.: The non-linear field theories of mechanics. In: Flugge, S. (ed.) Handbuch der Physik, vol. 3. Springer, Berlin (1965)
39. Reissner, E.: A further note on finite-strain force and moment stress elasticity. Z. Angew. Math. Phys. **38**, 665–673 (1987)
40. Pietraszkiewicz, W., Eremeyev, V.A.: On natural strain measures of the non-linear micropolar continuum. Int. J. Solids Struct. **46**, 774–787 (2009)
41. Germain, P.: The method of virtual power in continuum mechanics, part 2: microstructure. SIAM J. Appl. Math. **25**, 556–575 (1973)
42. Turco, E., et al.: Non-standard coupled extensional and bending bias tests for planar pantographic lattices. Part I: numerical simulations. Z. Angw. Math. Phys **67**(5), 122 (2016)
43. Turco, E., Barcz, K., Luigi Rizzi, N.: Non-standard coupled extensional and bending bias tests for planar pantographic lattices. Part II: comparison with experimental evidence. Z. Angw. Math. Phys. **67**(5), 123 (2016)
44. Auffray, N., dell'Isola, F., Eremeyev, V., Madeo, A., Rosi, G.: Analytical continuum mechanics á Hamilton–Piola: least action principle for second gradient continua and capillary fluids. Mech. Math. Solids (MMS) **20**(4), 375–417 (2015)
45. dell'Isola, F., Andreaus, U., Placidi, L.: At the origins and in the vanguard of peridynamics, non-local and higher gradient continuum mechanics. An underestimated and still topical contribution of Gabrio Piola. Mech. Math. Solids (MMS) **20**(8), 887–928 (2015)
46. Boutin, C., dell'Isola, F., Giorgio, I., Placidi, L.: Linear pantographic sheets: asymptotic micro–macro models identification. Math. Mech. Complex Syst. **5**(2), 127–162 (2017). https://doi.org/10.2140/memocs.2017.5.127
47. Spagnuolo, M., Barcz, K., Pfaff, A., dell'Isola, F., Franciosi, P.: Qualitative pivot damage analysis in aluminum printed pantographic sheets: numerics and experiments. Mech. Res. Commun. **83**, 47–52 (2017)
48. dell'Isola, F., Steigmann, D.J., Della Corte, A.: Synthesis of fibrous complex structures: designing microstructure to deliver targeted macroscale response. Appl. Mech. Rev. **67** (6), 060804, 21 pages (2016)
49. Turco, E., Golaszewski, M., Cazzani, A., Rizzi, N.L.: Large deformations induced in planar pantographic sheets by loads applied on fibers: experimental validation of a discrete Lagrangian model. Mech. Res. Commun. **76**, 51–56 (2016)
50. Abali, B.E., Muller, W.H., dell'Isola, F.: Theory and computation of higher gradient elasticity theories based on action principles. Arch. Appl. Mech. **87**, 1495–1510 (2017)
51. Cuomo, M., dell'Isola, F., Greco, L.: Simplified analysis of a generalized bias-test for fabrics with two families of inextensible fibres. Z. Angw. Math. Phys. 39 pages. https://doi.org/10.1007/s00033-016-0653-z (2016)
52. Abali, B.E.: Technical University of Berlin, Institute of Mechanics, Chair of Continuums Mechanics and Material Theory. Computational Reality. http://www.lkm.tu-berlin.de/ComputationalReality/ (2017)
53. Alnaes, M.S., Blechta, J., Hake, J., Johansson, A., Kehlet, B., Logg, A., Richardson, C., Ring, J., Rognes, M.E., Wells, G.N.: The FEniCS Project Version 1.5. Arch. Numer. Softw. **3**, 9–23 (2015). https://doi.org/10.11588/ans.2015.100.205532015